The Journal of Neuroscience, January 15, 1999, *19*(2):747–758

Dynamic Potassium Channel Distributions during Axonal Development Prevent Aberrant Firing Patterns

Ian Vabnick,[1] James S. Trimmer,[3] Thomas L. Schwarz,[4] S. Rock Levinson,[5] Dipesh Risal,[1] and Peter Shrager[1,2]

Departments of [1]Biochemistry and Biophysics and [2]Neurobiology and Anatomy, University of Rochester Medical Center, Rochester, New York 14642, [3]Department of Biochemistry and Cell Biology, State University of New York, Stony Brook, New York 11794, [4]Department of Molecular and Cellular Physiology, Beckman Center, Stanford University, Stanford, California 94305, and [5]Department of Physiology, University of Colorado, Denver, Colorado 80262

The distribution and function of Shaker-related K^+ channels were studied with immunofluorescence and electrophysiology in sciatic nerves of developing rats. At nodes of Ranvier, Na^+ channel clustering occurred very early (postnatal days 1–3). Although K^+ channels were not yet segregated at most of these sites, they were directly involved in action potential generation, reducing duration, and the refractory period. At ~1 week, K^+ channel clusters were first seen but were within the nodal gap and in paranodes, and only later (weeks 2–4) were they shifted to juxtaparanodal regions. K^+ channel function was most dramatic during this transition period, with block producing repetitive firing in response to single stimuli. As K^+ channels were increasingly sequestered in juxtaparanodes, conduction became progressively insensitive to K^+ channel block. Over the first 3 weeks, K^+ channel clustering was often asymmetric, with channels exclusively in the distal paranode in ~40% of cases. A computational model suggested a mechanism for the firing patterns observed, and the results provide a role for K^+ channels in the prevention of aberrant excitation as myelination proceeds during development.

Key words: potassium channels; node of Ranvier; Schwann cell; myelin; axons; development

The function of myelinated axons is dependent on a very heterogeneous distribution of ion channels, as well as a complex interaction of glial and axonal elements. In all known adult myelinated fibers, Na^+ channels are localized at high density within the nodal gap and are responsible for the upstroke of the action potential. In amphibian axons, voltage-dependent K^+ channels are likely to be colocalized with Na^+ channels, because their outward currents are recorded from nodes under voltage clamp and contribute to the repolarization of action potentials (Dodge and Frankenhaeuser, 1958; Schmidt and Stampfli, 1966; Hille, 1967). In normal mammalian PNS fibers, on the other hand, voltage-dependent K^+ currents are absent from nodes (Chiu et al., 1979), and their role in axons has thus been unclear. Chiu and Ritchie (1981, 1982) found that after acute disruption of myelin with lysolecithin, delayed rectifier K^+ currents appeared, suggesting a paranodal or internodal origin. It was later demonstrated that heteromultimers of the Shaker K^+ channel α subunits Kv1.1 and Kv1.2 and the cytoplasmic Kvβ_2 subunit, cluster in juxtaparanodal zones, internodal regions just beyond the paranodes (Wang et al., 1993; Mi et al., 1995; Rhodes et al., 1997). Both Na^+ channels and delayed rectifier K^+ channels are also present throughout the internode but at low density (Chiu and Ritchie, 1982; Shrager, 1987, 1988, 1989). Smart et al. (1998) recently demonstrated that genetic deletion of Kv1.1 resulted in hyperexcitability in CNS axons, as well as changes in the falling phase and refractory period of sciatic nerve action potentials. Finally, beyond their axonal segregation, K^+ channels are differentially distributed within neuronal somata, dendrites, and terminals (Sheng et al., 1992, 1994).

These various features of axonal structure do not appear simultaneously during development. Passive electrical properties change as glial cells adhere and ensheathe fibers, ultimately forming compact myelin with mature paranodes. Na^+ channels initially cluster in the axolemma adjacent to the edges of myelinating Schwann cell processes. As Schwann cell processes grow longitudinally, Na^+ channel clusters are reorganized into nodes of Ranvier (Dugandzija-Novakovic et al., 1995; Vabnick et al., 1996). Conduction velocity increases by up to two orders of magnitude during this time (Ziskind-Conheim, 1988; Vabnick and Shrager, 1998).

Despite these rather extensive alterations in structure, action potential propagation must be continually reliable and stable. Voltage-dependent K^+ channels can strongly influence conduction, even causing complete block if they are expressed in inappropriate locations. After demyelination, juxtaparanodal K^+ channels are no longer electrically isolated. Application of the K^+ channel blocking drug 4-aminopyridine (4-AP), which is without effect on normal fibers, significantly increases excitability, a finding of considerable clinical interest (Sherratt et al., 1980; Polman and Hartung, 1995; Schwid et al., 1997; Rasband et al., 1998). However, K^+ channel block restores conduction in some demyelinated fibers but induces repetitive firing in others (Burchiel and Russell, 1985; Baker and Bostock, 1992), perhaps by enabling reentry depolarization of paranodal regions (Chiu and Ritchie, 1981, 1984). It is thus important to understand the relationship

Received Sept. 10, 1998; revised Oct. 29, 1998; accepted Oct. 29, 1998.

This work has been supported by National Institutes of Health Grants NS17965, NS34383, and NS34375 and National Multiple Sclerosis Society Grant RG-2687. We thank Dr. Michael Hines for modification of the Neuron program and Matthew N. Rasband for comments on this manuscript. Katia Kazarinova helped with model calculations. Ms. Ellen Brunschweiger provided excellent technical assistance.

Correspondence should be addressed to Dr. Peter Shrager, Department of Neurobiology and Anatomy, Box 603, Room 4–5428, University of Rochester Medical Center, 601 Elmwood Avenue, Rochester, NY 14642.

between excitability and axonal K^+ channel organization. We find here that during the early postnatal period K^+ channels are essential for stable axonal conduction, and they are extensively redistributed to serve this function.

MATERIALS AND METHODS

Primary antibodies. Polyclonal anti-Kv1.1 antibodies were raised in rabbits against the C-terminal sequence EDMNNSIAHYRQANIRTG. The peptide was synthesized at the Beckman Center (Stanford University, Stanford, CA) and coupled to porcine thyroglobulin. Immunization, serum collection, and purification were as described previously (Mi et al., 1995). Mouse monoclonal anti-Kv1.1 antibody K20/78 was produced by immunization with the rat C-terminal peptide CEEDMNNSIAHYRQANIRTG (Quality Controlled Biochemicals, Hopkintown, MA) conjugated to either keyhole limpet hemocyanin (KLH) or bovine serum albumin (Bekele-Arcuri et al., 1996). Labeling patterns with the polyclonal and monoclonal anti-Kv1.1 antibodies were identical, and the choice was dependent on the antibody type used for double labeling. The mouse monoclonal anti-Kv1.2 antibody K14/16 (Bekele-Arcuri et al., 1996; Shi et al., 1996) was produced by immunization with a glutathione-*S*-transferase (GST) fusion protein containing amino acids 428–499 of rat Kv1.2. K14/16 binds to a synthetic peptide corresponding to amino acids 463–480 of Kv1.2. The mouse monoclonal anti-Kvβ_2 antibody K17/70 (Bekele-Arcuri et al., 1996; Rhodes et al., 1996) was produced by immunization with a GST fusion protein containing the entire 367 amino acid rat Kvβ_2 polypeptide. K17/70 binds to a synthetic peptide corresponding to amino acids 1–17 of Kvβ_2. Hybridomas were grown in Balb/c mice for production of ascites fluid as described previously (Trimmer et al., 1985). Immunoglobulins were purified by ammonium sulfate precipitation, followed by DEAE chromatography (Trimmer et al., 1985). Monoclonal antibodies against myelin associated glycoprotein (MAG) were a kind gift of Dr. Melitta Schachner (Zentrum fur Molekulare Neurobiologie, Hamburg, Germany) and were prepared by immunization with affinity-purified glycoproteins carrying the L2 epitope from chicken brain (Poltorak et al., 1987). The IgG antibody was obtained after fusion of the mouse myeloma clone P3X63Ag8.653, with spleen cells from immunized mice. The polyclonal anti-Na^+ channel antibody was raised against a highly conserved segment (TEEQKKYYNAMKKLGSKK) located between domains III and IV in the vertebrate Na^+ channel α subunit. The peptide, with a C-terminal cysteine, was synthesized at the University of Colorado Medical School institutional facility (Denver, CO) and was conjugated to maleimide-activated KLH. Antibodies were affinity purified using the immunizing peptide coupled to a Sulfolinked column (Pierce, Rockford, IL).

Immunocytochemistry. Procedures were similar to those used in earlier studies on developing and remyelinating nerve (Vabnick et al., 1996; Rasband et al., 1998). The animal was killed, and sciatic nerves and/or dorsal and ventral roots were dissected, desheathed, and dissociated in collagenase (3 mg/ml) for 10–20 min at room temperature (RT). One to 3 mm sections of the tibial branch were teased and attached to coverslips precoated with spots of Cell Tac (Collaborative Research, Bedford, MA). The tissue was fixed in 4% paraformaldehyde, pH 7.2, for 30 min at RT, washed in 0.05 M phosphate buffer (PB), pH 7.4, and air dried. Alternatively, in some experiments animals were deeply anesthetized and perfused with 4% paraformaldehyde in 0.1 M PB. The sciatic nerve was then dissected and post-fixed in 4% paraformaldehyde for 4 hr at 4°C, rinsed in 0.1 M PB for 10 min, incubated overnight in 20% sucrose, and again in 30% sucrose overnight. The nerve was then frozen in OCT mounting medium (Miller, Inc.) and cut in 30-μm-thick sections. These sections were then spread on gelatin-coated slides, fixed again for 10 min in 4% paraformaldehyde, rinsed in 0.05 M PB, and allowed to dry.

Both teased axons and cryosections were exposed to a solution containing 45 ml of 0.1 M PB, 150 μl of Triton X-100, and 5 ml of goat serum (PBTGS) for 2 hr. All subsequent solutions used the PBTGS mixture for dilutions or washing. Primary antibodies were applied for 15 hr at RT. For rabbit polyclonal antisera, the secondary labeling consisted of biotinylated goat anti-rabbit Fab_2' (1:200, 1 hr), followed by Extravidin-fluorescein isothiocyanate (1:200, 1 hr). For monoclonal antibodies, the fluorescent ligand was goat anti-mouse tetramethyl rhodamine isothiocyanate. In most experiments, axons were double labeled by applying one primary antibody and its secondary antibody, followed by the second series. Preparations were washed three times with PBTGS after each reagent. After immunolabeling, coverslips were washed sequentially in PBTGS, 0.1 M PB, and 0.05 M PB for 5 min each. Tissue preparations were air dried and mounted on slides for visualization under a Nikon Microphot-SA fluorescence microscope fitted with a Dage MTI (Michigan City, IN) SIT 68 camera. Images were captured and stored in a computer for later analysis. Preabsorption of Na^+ and Kv1.1 antibodies with peptide antigens eliminated immunolabel (Dugandzija-Novakovic et al., 1995; Rasband et al., 1998).

We required criteria for designating K^+ channel immunoreactivity as nodal, paranodal, or juxtaparanodal. The nodal gap was readily identified by either Na^+ channel labeling or MAG staining of paranodes. The point at which the paranodal loops end and the juxtaparanodes begin cannot be determined at the light level in immature fibers. We used published data to estimate paranodal lengths of 4–8 μm in the adult and 2–4 μm in early development (Allt, 1969; Tao-Cheng and Rosenbluth, 1982, 1983; Yamamoto et al., 1996). K^+ channel immunoreactivity was considered paranodal if it was <5 μm from a node. In adult fibers, the axon diameter increases sharply to the internodal value at the border of the paranode, and label within this expanded zone (and >2 μm from the node) was thus considered to be juxtaparanodal. By the end of the first postnatal week, MAG is expressed at elevated levels in the terminal loops and thus demarcates the paranodes. Double labeling with anti-MAG antibodies beyond postnatal day 6 (P6) confirmed the validity of the above criteria and was also used in many experiments as an additional determinant of localization. In cases in which K^+ channel immunoreactivity was present in two regions, i.e., nodal/paranodal or paranodal/juxtaparanodal, the site was included in both categories. Throughout the paper, the term "site" refers to nodal regions, including the nodal gap, paranodes, and juxtaparanodes.

Suction electrode recording. Rat sciatic nerves were dissected and desheathed as above and placed in Locke's solution containing (in mM): NaCl 154, KCl 5.6, $CaCl_2$ 2, D-glucose 5.6, and HEPES 10, pH 7.4. The floor of the nerve chamber was constructed from glass coated on the outside surface with indium tin oxide, allowing heating with an electric current. This provided a highly uniform bath temperature without the need for mechanical agitation. A thermistor and feedback electronics controlled the temperature to ± 0.5°C. Each end of the nerve was drawn into a glass capillary electrode with a constricted orifice. Brief (50 μsec) stimulating pulses were applied to the proximal (toward spinal cord) electrode, and the compound action potential was recorded from the distal end. With the stimulus parameters then set, the distal end was removed from its electrode and dissociated in collagenase (3 mg/ml) for 5–30 min until the tips of individual fibers could be visualized. This enzymatic procedure has been shown not to affect compound action potentials (Shrager, 1987). A single axon was then drawn into a broken microelectrode (2–15 μm inner diameter) for a distance of 25–100 μm. After a stimulus, signals were recorded with an Axopatch 200A amplifier (Axon Instruments, Foster City, CA) in current-clamp mode (with steady-state current set to zero) and then passed through an alternating current amplifier (Warner DP301). Amplitude corrections for much of the variation in seal resistance (R_{seal}) at the recording pipette were made by the method of Stys et al. (1991), except for a few cases in which R_{seal} was <1 MΩ. The primary information, however, is in the shape and timing of signals. Action potentials were digitized and stored in a computer for later analysis.

The influence of K^+ channels was tested by applying one of several blocking drugs. Tetraethylammonium ion (TEA) (10 mM) or dendrotoxin I (DTX-I) (100 nM; Calbiochem, San Diego, CA) were typically applied first, because effects were readily reversed on washing. 4-AP (1 mM) was then added. In a few experiments, washout of 4-AP was attempted, with partial or complete reversal of effects over ~45 min. Responses after application of these drugs were observed for at least 10 min to ensure that the effect was maximal.

Computational model. Using the Neuron modeling computer program (www.neuron.yale.edu/neuron) (Hines and Carnevale, 1997), we designed an equivalent circuit for a P16 axon. The fiber included 21 nodes and 20 internodes. Nodal, paranodal, juxtaparanodal, and internodal zones were defined as shown in the sketch within Table 1. Morphological and electrical parameters were obtained from several published sources and are listed in Table 1. The number of myelin lamellae covering paranodal segments was decreased linearly toward the node, corresponding to the geometry of the terminal loops. The length of the paranode was calculated by multiplying the number of myelin layers by a terminal loop periodicity of 0.15 μm (Rosenbluth, 1988). K^+ channel permeabilities were estimated by taking the ratio of peak K^+ conductance to peak Na^+ conductance after paranodal retraction (Chiu and Ritchie, 1981) and multiplying by the nodal Na^+ channel permeability. The ratio of

Table 1. Parameters for the neuron model

Parameter	Ranvier node	Paranode	Juxtaparanode	Internode	Units
Maximum Na^+ channel permeability	0.008[a]	0.0[b]	0.0[b]	0.0003[c]	cm/sec
Maximum K^+ channel permeability	0.0[b]	0.0001	0.0004	0.00005	cm/sec
Leakage conductance	0.03[a]	0.001	0.001	0.001	S/cm^2
Axonal membrane capacitance	2[a]	1	1	1	$\mu F/cm^2$
Schwann cell/myelin membrane conductance[d]		0.0025	0.0025	0.0025	S/cm^2
Schwann cell/myelin membrane capacitance[d]		1	1	1	$\mu F/cm^2$
Axoplasmic resistivity[c]	110	110	110	110	Ωcm
Bath resistivity[f]	80	80	80	80	Ωcm
Resting membrane potential	−80	−80	−80	−80	mV
Myelin layers[g]	0	1–44	44	44	
Axon diameter[g]	2.2	2.2	2.2	2.2	μm
Glial–axon intercellular gap[h]		0.002–0.01	0.02	0.02	μm
Section axial length	1[g]	6.6	5[g]	220[g]	μm

[a](Frankenhaeuser and Huxley, 1964)
[b](Chiu and Ritchie, 1981)
[c](Shrager, 1987)
[d](Strichartz et al., 1984)
[e](Stampfli, 1952)
[f](Milton et al., 1985)
[g](Webster, 1971)
[h](Tao-Cheng and Rosenbluth, 1983)

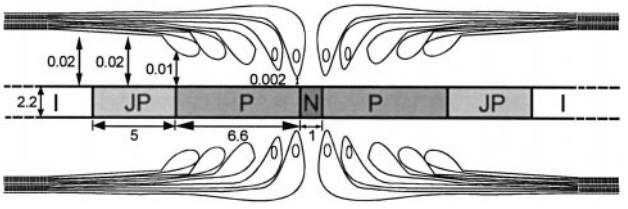

As shown in the sketch, the axon is divided into four zones: N, nodal; P, paranodal; JP, juxtaparanodal; and I, internodal. Dimensions are in micrometers.

internodal to maximal paranodal or juxtaparanodal K^+ channel permeability per unit area is close to the value estimated by Roper and Schwartz (1989). To mimic the maturation of the paranodal axoglial junctions (Tao-Cheng and Rosenbluth, 1983; Yamamoto et al., 1996), we constricted the axoglial gap linearly starting at 20 Å nearest the node and increasing to 90–120 Å at the paranodal/juxtaparanodal border (Table 1, sketch). K^+ channels were excluded from paranodal regions with a gap of 20 Å, i.e., zones of mature junctions. The axon was stimulated with a pulse of current (100 nA, 50 μsec) at the first node of Ranvier. The last internode was placed inside a simulated suction electrode with a R_{seal} of 10 MΩ. The extracellular voltage was calculated at the midpoint of this internode.

RESULTS

K^+ channel localization during early postnatal development

At birth, rat sciatic axons had almost no myelin, and neither Na^+ nor K^+ channels were detected by immunocytochemistry. As will be shown later, conduction in these nerves is slow and is likely to be mediated by channels diffusely distributed below immunodetectable levels. Over the first few days, myelination proceeded rapidly. Clusters of Na^+ channels were readily detected at gaps between Schwann cell processes, but Kv1.2 and Kv1.1 immunoreactivity was absent in 90% of these sites (Fig. 1*A*,*B*, respectively). The Na^+ channel clusters at this stage were either binary (Fig. 1*A*) or uniform and broad (Fig. 1*B*), typical of early node formation (Vabnick et al., 1996). By P6–P9, nodal Na^+ channel clusters were more focal, but in 80% of these cases, K^+ channels remained undetectable (Fig. 1*C*). However, K^+ channel immunoreactivity was seen in the other 20% of fibers at this stage, usually within paranodes (Fig. 1*D*). Thus, Na^+ and K^+ channels differ both temporally and spatially in clustering during early development. The segregation of Na^+ channels precedes that of K^+ channels and advances to a secondary stage before the density of Kv1.1 or Kv1.2 channels is detectable.

By the second postnatal week, >50% of sites had intense Kv1.1 and Kv1.2 immunoreactivity within paranodal regions. However, almost half of the K^+ channel-immunopositive locations were labeled asymmetrically. Notably, at these sites, the distal paranode was invariably the one with K^+ channels. Figure 1*E* illustrates this organization for Kv1.2 at P13. This pattern was transient, and by the end of the third postnatal week, K^+ channel labeling had the symmetry characteristic of adult fibers. (As will be shown shortly, Kv1.1 and Kv1.2 were colocalized at all stages, and they are thus discussed interchangeably here.) K^+ channel immunofluorescence shifted gradually toward the internode over the next several weeks. At this stage of development, there was a mixed population of Kv1.1-immunopositive sites in which at some locations labeling extended across both paranodes and juxtaparanodes, whereas at others, channels were exclusively juxtaparanodal. Eventually, the majority of sites contained K^+ channels segregated only within the juxtaparanodal zones, as can be seen in Figure 1*F* at P61.

Between P6 and P8, Kv1.1 and Kv1.2 immunofluorescence was present *within the nodal gap* at ~20% of sites, although typically at low intensity. Figure 1, *G* and *H*, illustrates nodes of Ranvier in two axons at P7, labeled with antibodies against Kv1.2 (*G*) and Na^+ (*H*) channels. It can be seen that one of these sites (*arrowheads*) included a Kv1.2 cluster (*G*) that colocalized with Na^+ channels (*H*). The distal paranode at this site (*G*) had diffuse K^+ channel labeling that appeared to be separated from the nodal cluster by a small gap. In the second node of Ranvier seen in Figure 1, *G* and *H*, Kv1.2 label was not detected, and as noted above, this was true in the majority of cases. Nodal Kv1.1 and Kv1.2 distributions disappeared rapidly and were virtually absent by the end of the first postnatal week.

At early stages, K^+ channels were frequently found organized in several transverse bands or spirals. Figure 1*I* illustrates one such region, in a P21 axon. MAG is expressed by Schwann cells after they reach an overlapping (~1.5 wraps) ensheathement, indicating a commitment to myelination (Martini and Schachner,

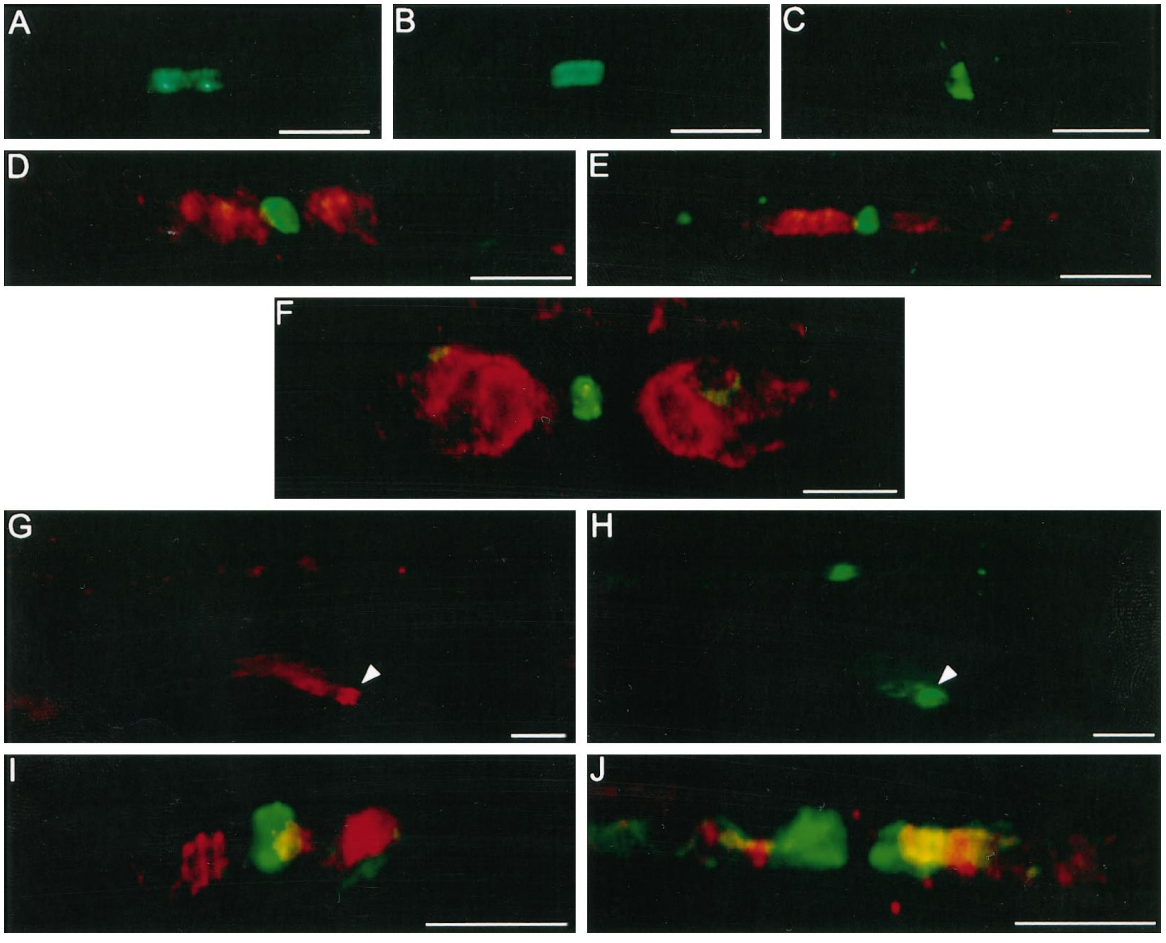

Figure 1. The distribution of K^+ channels in developing axons. All preparations were double stained with antibodies to K^+ (*red*) and Na^+ (*A–I*, *green*) channels or MAG (*J*, *green*). *A*, *B*, Lack of K^+ channel immunoreactivity (*A*, Kv1.2; *B*, Kv1.1) at P3. Na^+ channel clusters were either binary (*A*) or broad (*B*). *C*, Focal Na^+ channel cluster with no detectable Kv1.1 channels at P7. *D*, Diffuse Kv1.1 channel immunoreactivity within paranodes, adjacent to Na^+ channel clusters (P9). *E*, Asymmetric Kv1.2 localization predominantly in the distal paranode at P13. *F*, Juxtaparanodal Kv1.1 immunoreactivity at P61. Note sharp increase in axonal diameter in this region. *G*, *H*, K^+ channel clustering within the nodal gap. Two axons double labeled for Kv1.2 (*G*) and Na^+ (*H*) channels. In the *bottom* fiber, a node (*arrowhead*) is characterized by colocalization of these channels. The distal paranode at this site is also immunopositive for Kv1.2, although separated from the nodal cluster by a small gap. In the *top* axon, only Na^+ channel immunoreactivity is strong. *I*, Organization of Kv1.2 channels in transverse bands resembling helices at P21. *J*, Another site with K^+ channels (Kv1.1) in transverse bands double labeled for MAG (*green*). The partial overlap (*yellow*) indicates that these channels are both paranodal and juxtaparanodal (P14). Scale bars, 10 μm.

1986). MAG is initially rather uniformly distributed over the Schwann cell surface, but as myelination proceeds, this molecule is increasingly sequestered within terminal loops and other cytoplasm-containing regions. MAG labeling thus helps in defining the extent of the paranodes. In Figure 1*J*, the region of overlap of Kv1.1 with MAG (yellow) shows that the K^+ channel bands were within these latter zones, associated with the paranodal termini furthest from the node. In this example K^+ channel immunoreactivity extended beyond the MAG-positive zone into the juxtaparanode. The banded–spiral pattern of Kv1.1 and Kv1.2 channels was reminiscent of the regularly spaced terminal Schwann cell loops (Rosenbluth, 1988). However, the width of the K^+ channel bands was typically ~0.4 μm, and the periodicity was ~1.2 μm. Mature terminal loops are 0.1–0.2 μm in width and are usually tightly packed (Rosenbluth, 1988). On the other hand, lakes of intramembranous particles up to 0.4 μm in width have been seen in freeze-fracture of paranodal regions in ~40% of spinal roots (Fields et al., 1986). At later stages of development, as K^+ channels became increasingly sequestered at juxtaparanodal zones, there was minimal overlap between K^+ channels and MAG, and the banded appearance became very rare.

Kv1.1 and Kv1.2 subtypes were colocalized in most axons at all stages of development studied. Figure 2, *A* and *B*, illustrates a node of Ranvier at P13 with overlapping clusters of Kv1.2 and Kv1.1 subunits, respectively, at the distal paranode. A node at P40 at which the juxtaparanodal regions were immunopositive for both channels is shown in Figure 2, *C* and *D*. Even at the earliest times of detection of K^+ channel clustering (P6–P9), Kv1.1 and Kv1.2 were almost invariably coexpressed in paranodal regions. The K^+ channel subunit Kvβ_2 promotes surface expression and colocalizes with Shaker-type α subunits in rat brain juxtaparanodal regions (Shi et al., 1996; Rhodes et al., 1997). This association is present in developing sciatic nodes of Ranvier also. Figure 2, *E* and *F*, illustrates a node of Ranvier at P13, with asymmetric but overlapping paranodal staining of Kvβ2 (*E*) and Kv1.1 (*F*). When both antigens tested (Kv1.1/Kv1.2 or Kv1.1/Kvβ_2) were immunopositive at a particular region, the overlap was typically very strong, as in the above examples. At a small number of sites, however, fluorescence from one of the two antibodies tested was absent. It could not be determined whether these locations truly lacked the tested subunit or whether there was a technical failure of the antibody labeling. In remyelinating axons, ~15% of sites

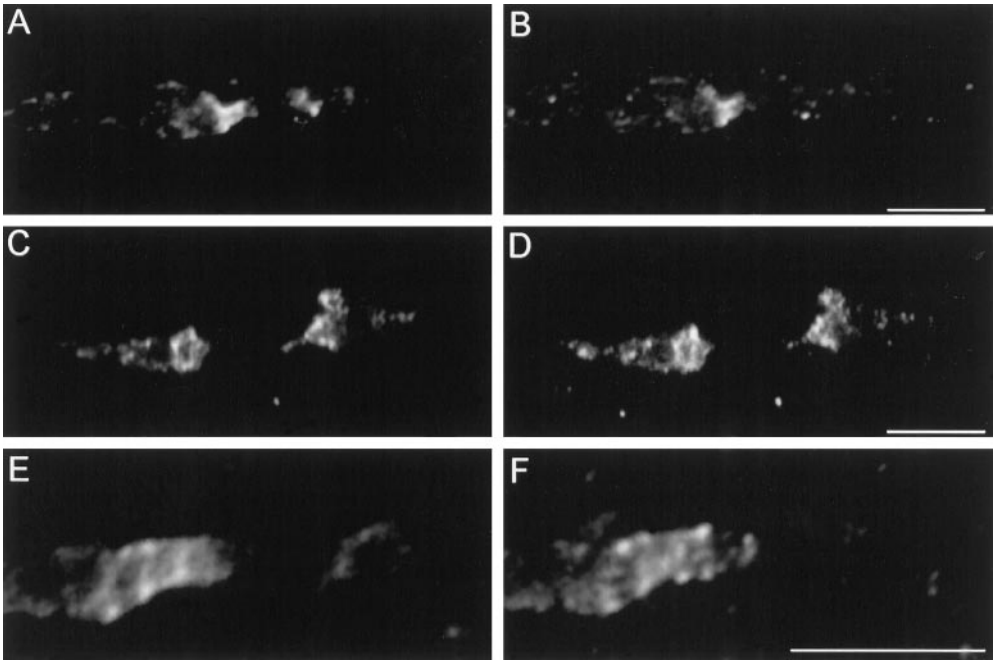

Figure 2. Colocalization of K^+ channel subunits at developing paranodes and juxtaparanodes. *A*, A node with an asymmetric distribution of Kv1.2 subunits at P13. *B*, Colocalization of Kv1.1 at the same site as in *A*. *C*, *D*, Juxtaparanodal immunoreactivity of Kv1.2 (*C*) and Kv1.1 (*D*) at P40. *E*, Kvβ_2 subunits at the distal side of a node at P13. *F*, The site in *E* double labeled for Kv1.1 α subunits. Scale bars, 10 μm.

were positive for Kv1.1 and negative for Kv1.2 (Rasband et al., 1998), but in the developing fibers the immunonegative subunit varied.

The frequency of occurrence of several K^+ channel patterns is plotted in Figure 3*A*. Because Kv1.1 and Kv1.2 immunofluorescence was the same at all stages examined, only results for the former are shown. The classification included (1) sites with no detectable Kv1.1 signal (▼); (2) nodes at which Kv1.1 and Na^+ channel immunofluorescence overlapped, with or without additional paranodal label (■); (3) paranodal regions, defined as Kv1.1 label adjacent to a node but not present within it (●); and (4) juxtaparanodal zones, defined by Kv1.1 immunoreactivity >2 μm from nodal Na^+ channels (▲). Despite our attempts at defining criteria for classification, it was not possible to distinguish between paranodal and juxtaparanodal label in many cases. During P23–P61, a significant percentage of sites had K^+ channel immunoreactivity that appeared to extend through both regions, and these were counted in both groups (see Materials and Methods). Most features of these curves were measurable with accuracy; the major uncertainty is in the timing of the initial appearance of juxtaparanodal channels, which may be shifted earlier. Figure 3*A* shows that at birth Kv1.1 was undetectable. The earliest appearance of this channel in clusters was within the nodal gap, and that configuration represented ~20% of the sites examined by P6. However, this localization was highly transient, and the percentage of sites with nodal K^+ channels dropped nearly to zero after P9. Approximately 90% of these sites had associated paranodal immunofluorescence. The rate of appearance of paranodal channels rose rapidly during the second postnatal week, reaching a maximum frequency of ~75%. The percentage of sites with juxtaparanodal Kv1.1 clusters increased steadily over weeks 2–4, and this became the predominant adult form. The behavior of the paranodal and juxtaparanodal data suggest that sites with the former localization progress to the latter. The question of whether K^+ channels begin within the nodal gap at all sites is addressed in Discussion. Up to the maximum age examined, ~10% of sites remained immunonegative for Kv1.1 or Kv1.2. We found that during development K^+ channel clusters were not detected in axons <2 μm in diameter.

The frequency of occurrence of sites with K^+ channels detected only at the distal paranode during development is plotted in Figure 4, ●. Also shown is the frequency of symmetrical labeling (■). The data suggest that at about half of the developing nodal regions K^+ channels cluster preferentially at the distal paranode during the second postnatal week. However, this situation is transient, and over the succeeding week paranodes become symmetrically labeled at all such sites. A possible functional significance of the asymmetric expression is explored later using a computational model. During development, dorsal and ventral spinal roots respond differently to pharmacological block of K^+ channels (Bowe et al., 1985). However, we found no significant differences in Kv1.1/Kv1.2 organization among different roots (data not shown; examined at P8, P12, and P19). In contrast to the sciatic nerve, very few sites in spinal roots were labeled preferentially at one paranode at any stage examined.

Single fiber recording as a test for K^+ channel function

Longitudinal currents were measured from single axons at all stages of postnatal development. Even small premyelinated fibers at P0 could be drawn into suction electrodes with minimal mechanical stress. All-or-none action potentials were recorded before and after adding blocking drugs as a test of K^+ channel participation in signal generation and propagation. Over the first week, during early node formation and Na^+ channel clustering, 4-AP had small but significant effects, slowing the falling phase of action potentials. This is evident in Figure 5 in which the biphasic undershoot present in the control trace (*A*) is absent after introduction of the drug (*B*). This change in shape was observed in ~90% of fibers from P0 through P8. This result indicates that although Kv1.1/Kv1.2 subunits are not detectable by immunocytochemistry at this stage, K^+ channels (possibly including non-Shaker types) are present in the axolemma at low density and

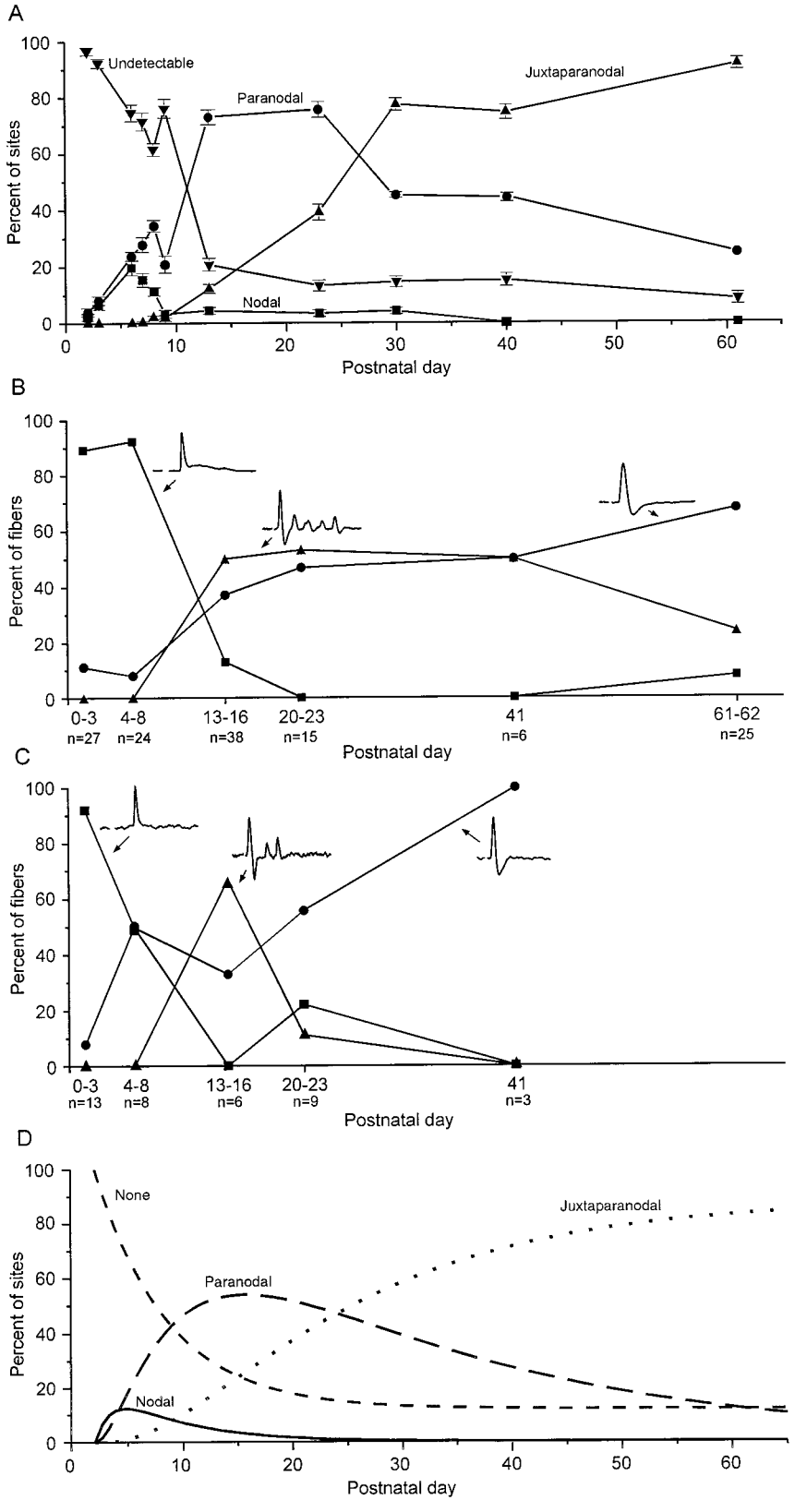

Figure 3. The variation in K^+ channel distribution and influence on electrical signals during development. *A*, Kv1.1 patterns. Sites were tallied by comparing loci of K^+ and Na^+ channel immunoreactivity and placed in the following categories: sites with undetectable Kv1.1 (▼); Kv1.1 colocalized with nodal Na^+ channel clusters (■); paranodal Kv1.1 (label adjacent to but not overlapping Na^+ channel) (●); and juxtaparanodal Kv1.1 immunofluorescence, >2 μm from a node (▲). *B*, Sensitivity to block as a measure of K^+ channel function at different developmental stages. Changes in single fiber waveforms at RT on introduction of 4-AP were classified as the following: monophasic (■); repetitive firing (▲); and biphasic as in the absence of drug (●). Results were grouped as noted on the abscissa. Recordings were made from a total of 97 fibers, with the numbers per group indicated below the abscissa. Because the number of fibers tested in each individual experiment was small (often only 1), error bars for percentages could not be calculated. *C*, Similar to *B* but at 37°C. *D*, Calculated levels of different K^+ channel distributions for a simple kinetic scheme: none → nodal → paranodal → juxtaparanodal. The rate constants for the three irreversible steps used in this fit were 0.15, 0.70, and 0.04 d^{-1}, respectively. In this plot, the four categories are mutually exclusive. If we allowed for sites with either nodal/paranodal or paranodal/juxtaparanodal overlapping immunoreactivity, then the paranodal curve would be effectively higher in amplitude, and the fit to the data in *A* would be improved.

function in action potential generation. During the second and third postnatal week, 4-AP induced more significant changes in the action potential waveform. After a single stimulus, axons fired repetitively, as shown at P20 in Figure 5*D*. The secondary responses were more prominent at lower temperatures, and the exact pattern in each fiber varied somewhat with successive stimuli. These multiple spikes were never seen in the absence of 4-AP. Spiking waveforms after K^+ channel block at this stage of devel-

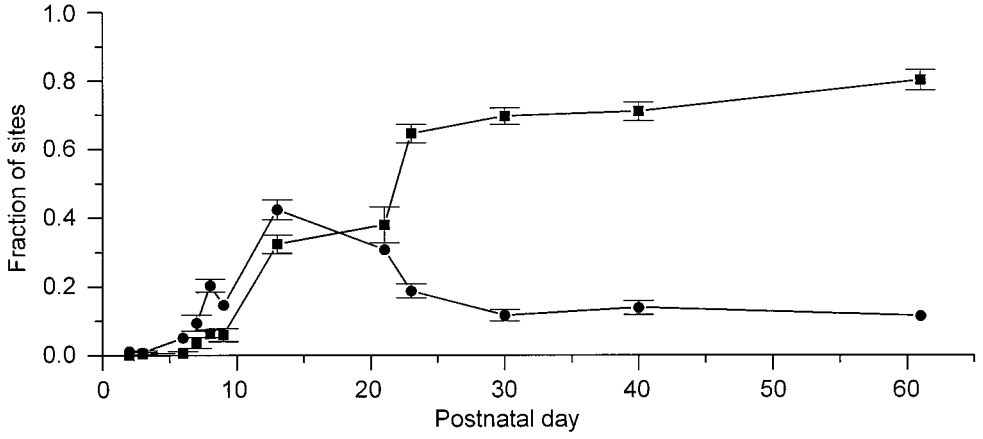

Figure 4. Asymmetrical distribution of K^+ channels. The fraction of sites with Kv1.1 either symmetrically distributed (■) or present exclusively in the distal paranode and juxtaparanode (●) are plotted versus postnatal day.

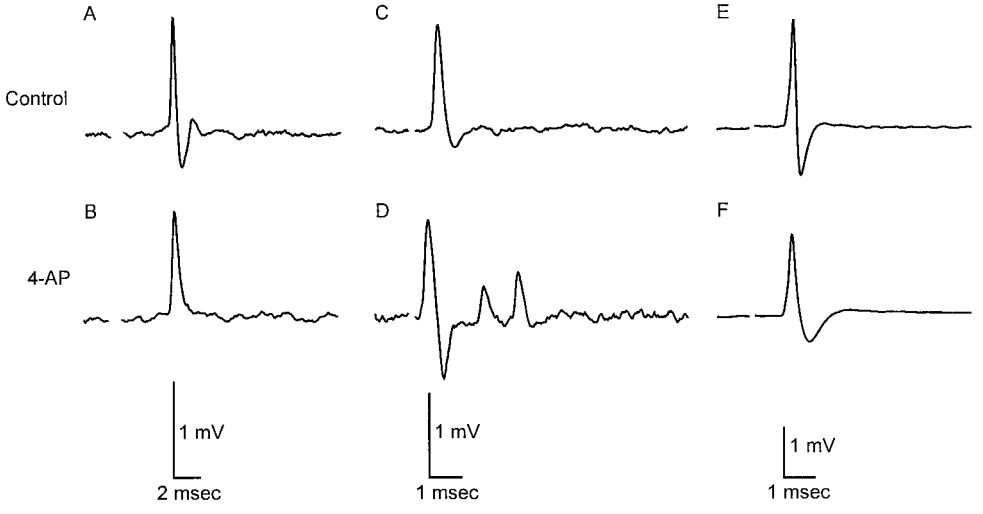

Figure 5. Sensitivity of propagating action potentials to K^+ channel block. *Traces* were derived from single fibers drawn into suction electrodes. Records are shown before (*A*, *C*, *E*) and after (*B*, *D*, *F*) introduction of 1 mM 4-AP in the bath. At P0, a typically biphasic recording (*A*) became monophasic, with loss of the negative phase indicating a slower repolarization in the presence of the drug (*B*). At P20, 4-AP induced repetitive firing in response to a single stimulus (*C*, *D*). There is relatively little change in waveform at P62, and the *trace* remained biphasic, indicative of rapid repolarization (*E*, *F*). Stimulus artifacts have been blanked. The time of stimulation is indicated by the start of the gap in each record. All records are at 37°C.

opment have been reported also by Kocsis et al. (1983). The bursting behavior remained through P41, but by P62, 4-AP had only small effects, as may be seen in Figure 5, *E* and *F*.

The electrical responses after exposure to 4-AP were divided in three categories: monophasic, repetitive firing, and biphasic, as represented by the traces in Figure 5, *B*, *D*, and *F*, respectively. The frequency of occurrence of each of these is plotted as a function of age in Figure 3, *B* (at RT) and *C* (at 37°C). These results are now compared with those for K^+ channel clustering. Monophasic recordings (■) represent over 90% of axons tested over the first postnatal week but then fall off rapidly. This coincides closely with the curve for axons with no detectable K^+ channel clusters in Figure 3*A*, ▼. The spiking response was transient and corresponds most closely to the localization of K^+ channels in paranodes (Fig. 3*A*, ●). Traces that remained biphasic in 4-AP rose in frequency over the period studied and thus corresponded most closely to the data for juxtaparanodal localization in Figure 3*A*, ▲. This comparison of electrophysiological results with immunocytochemistry suggests that voltage-dependent K^+ channels play important roles in signaling during early development.

The refractory period represents another important determinant of axonal function. As a measure of this property, three stimuli at equally spaced intervals were applied. The interstimulus interval was progressively shortened until the second response was blocked and could no longer be recovered, even with an increase in the stimulus amplitude. This is illustrated for a P6 axon in Figure 6, *A–D*. In normal Locke's solution, three stimuli at intervals of 2 msec result in three action potentials (Fig. 6*A*). When the interval is reduced to 1 msec, the second action potential is missing (Fig. 6*B*). After exposure to 1 mM 4-AP, the refractory period is much longer. At an interval of 8.5 msec, all spikes are present (Fig. 6*C*), but at 8 msec, the fiber is refractory (Fig. 6*D*). K^+ channel block thus increased the refractory period for this axon from <2 to 8 msec. The increase in refractory period with K^+ channel block was strong over the first postnatal week and then declined, disappearing at ~6 weeks. This could not, however, be quantitated rigorously, because over weeks 3–5 repetitive firing in the presence of 4-AP introduced uncertainties in the measurement of the refractory period. Multiple spikes were often present in the first response only, even when the primary action potential was generated in response to all three stimuli (Fig. 6*E*).

DTX-I has a more selective spectrum of targets than does 4-AP and blocks mouse Kv1.1, Kv1.2, and Kv1.6 channels selectively with IC_{50} values of 3.1, 0.13, and 9 nM, respectively (Swanson et al., 1990; Hopkins et al., 1994). At P0 and P1, four of six fibers tested were sensitive to DTX-I (100 nM). The records of Figure 7*A* came from one such axon and suggest a significant and reversible slowing of the falling phase of action potentials by this drug. Neither of two fibers at P6 and P7 exposed to 100 nM DTX-I were affected. Subsequent to addition of DTX-I, all of these axons were found to be sensitive to 4-AP. By P6–P7, access of the

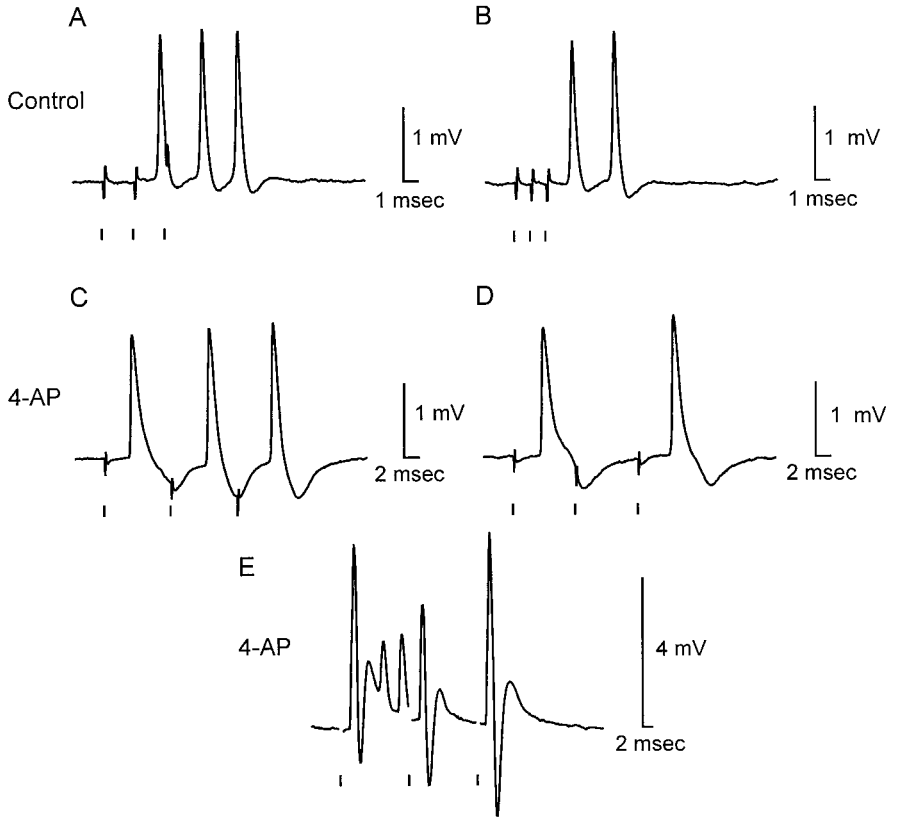

Figure 6. Measurement of the refractory period. In each record, three stimuli were applied at equal intervals (Δt). The *tic marks below* each *sweep* denote the times of stimulation. *A–D*, Signals from a P6 fiber. *A*, Locke's solution, Δt = 2 msec. *B*, Locke's solution, Δt = 1 msec. *C*, One millimolar 4-AP, Δt = 8.5 msec. *D*, One millimolar 4-AP, Δt = 8 msec. *E*, P16 axon, 1 mM 4-AP, Δt = 14 msec. Temperature for all *traces* was 37°C.

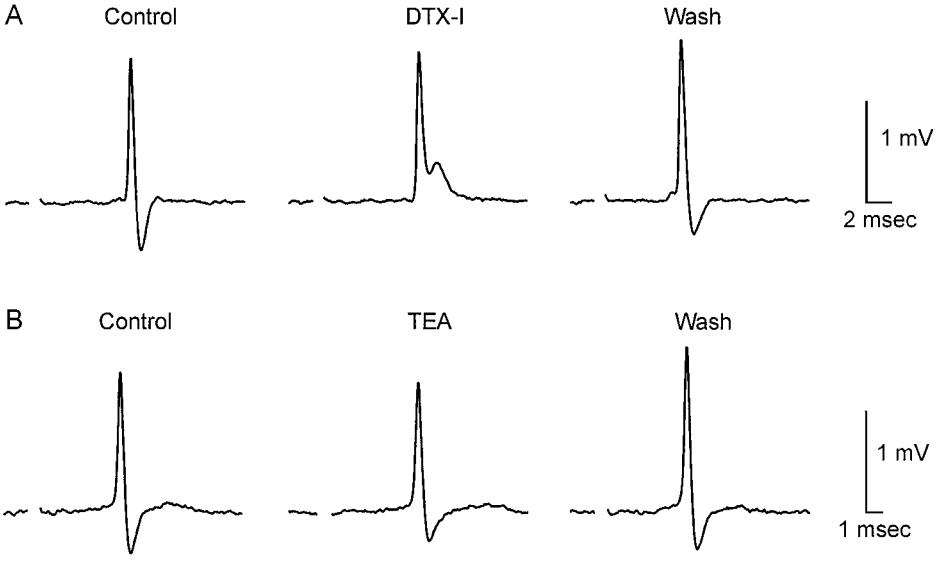

Figure 7. Response of early developing fibers to the K^+ channel blocking drugs DTX-I and TEA. *A*, One hundred nanomolar DTX-I added to the bath inverted the negative phase of the extracellular recording, suggesting a widening or plateau in the action potential. The change was reversible on washing (P0). *B*, Lack of response of a P1 axon to 10 mM TEA added to the Locke's solution. In this experiment, the R_{seal} was inadequate for normalization of amplitudes.

peptide toxin to paranodal channels may be restricted. TEA is a much more potent blocker of homomultimeric Kv1.1 channels (IC_{50} value of 0.3 mM) than Kv1.2 channels (IC_{50} values of 107–560 mM) (Grissmer et al., 1994; Hopkins et al., 1994). Heteromultimers are blocked with an IC_{50} value of ~10 mM (Hopkins et al., 1994). Only 3 of 24 fibers tested over P0–P61 had a significant response to this drug when applied at a concentration of 10 mM. In all other cases, the action potential waveform was only minimally affected (Fig. 7*B*). This result is consistent with the low sensitivity of internodal delayed rectifier K^+ currents to externally applied TEA (Chiu and Ritchie, 1981; Shrager, 1987).

Computational models of developing nerves

A computational model of a P16 axon was developed that reproduced as many details of morphology and ion channel distribution as are known and can be quantified (see Materials and Methods). This system was then used to test the role of K^+ channels in several physiological responses. In Figure 8*A*, the *sweep* on the *left* was calculated for an axon with paranodal/juxtaparanodal K^+ channels distributed symmetrically about each developing node. In the *trace* on the *right*, all K^+ channels were removed, simulating a response in 4-AP. There were multiple depolarizations in response to a single stimulus, comparable to records in Figure 5,

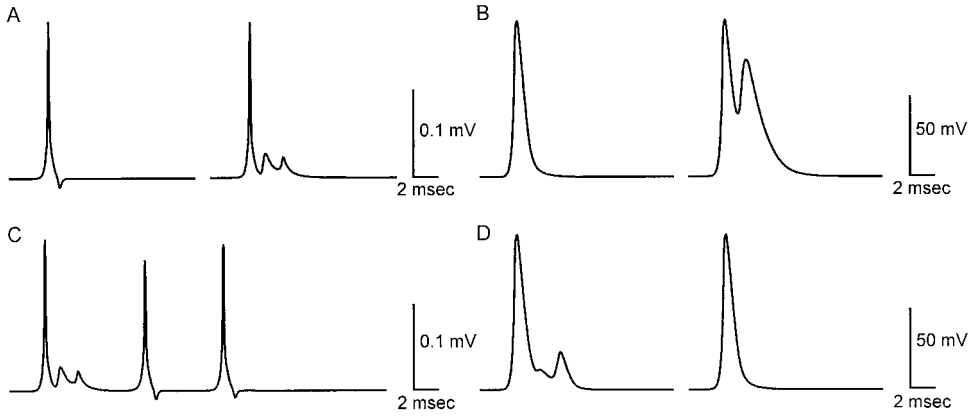

Figure 8. Computed action potentials as a test of K^+ channel function. *A*, *Left*, A calculated propagating action potential in a P16 axon as recorded by the simulated suction electrode. *Right*, After removal of the paranodal/juxtaparanodal K^+ channel clusters. *B*, Computed transmembrane potentials at a node outside the electrode for the same conditions as in *A*. *C*, Calculated suction electrode response to three stimuli applied at 7 msec intervals; K^+ channels blocked. *D*, *Left*, Computed transmembrane voltage with either proximal or distal paranode/juxtaparanode depleted of clustered K^+ channels. *Right*, After doubling the K^+ channel density on the populated side.

C and *D*. The *sweeps* in Figure 8*A* were calculated as extracellular potentials within a suction electrode to allow a comparison with experimental results. The model allowed a calculation of membrane potential as well, and this is plotted in Figure 8*B* for a node just outside the suction electrode, under the same conditions as in Figure 8*A*. With K^+ channels removed (*right*), there were two prominent peaks in the response. It was of interest that the relatively small secondary spikes detected by the extracellular electrode can represent large propagating signals outside the pipette. The low density of internodal Na^+ channels normally produced a current that was delayed relative to the peak nodal Na^+ current. Removal of these internodal Na^+ channels eliminated the repetitive firing (data not shown). The calculations thus suggest that the paranodal/juxtaparanodal K^+ channels normally act to suppress a reentry depolarization mediated by the internodal Na^+ channels in these immature fibers.

The model also reproduced several aspects of links between K^+ channels and the frequency dependence of developing fibers. In Figure 8*C*, three stimuli were applied to a model axon with no paranodal/juxtaparanodal K^+ channels, and extra spikes were present only in response to the first stimulus, a result similar to that seen in Figure 6*E* with 4-AP. The computed trace did, however, include a delay in the response to the second stimulus that was not seen in the experiment. Again, the internodal Na^+ channels are implicated in the repetitive firing, because inward current through these channels was much reduced in the second and third responses. The internodal channels remained inactivated, presumably because of long charging and discharging times of the internodal axolemma (Barrett and Barrett, 1982). It should be noted that the spatial separation of nodal and internodal Na^+ channels also had a significant effect on bursting behavior. Decreasing the size of the juxtaparanode or paranode resulted in the loss of the spiking response (data not shown). Further, if the paranodal periaxonal space were reduced below 90 Å, as seen at mature paranodes, K^+ channel block no longer resulted in repetitive firing. There was also an increase in the computed refractory period with block of K^+ channels, from 4 to 6.5 msec. Finally, we tested possible consequences of an asymmetrical distribution of K^+ channels. If the density of channels in either paranode/juxtaparanode were reduced to the internodal value, there was repetitive firing (Fig. 8*D*, *left sweep*). However, doubling the channel density in the populated side restored a normal response (Fig. 8*D*, *right sweep*). Thus, the restriction of K^+ channels to just one side can lead to instabilities, but this seems to be attributable primarily to the reduced total number of K^+ channels near a node and not to the asymmetry in the distribution.

As noted earlier, at ~20% of sites, K^+ channels were seen within the nodal gap at very early stages. This was of interest, because during the formation of new nodes of Ranvier in remyelinating axons these channels clustered first at this location and only later shifted into paranodal zones (Rasband et al., 1998). In developing axons, nodal K^+ channel immunoreactivity was relatively weak and was very transient, virtually disappearing by P9. Further, the percentage of sites with this expression pattern was significantly less than the 60% seen during remyelination. Nonetheless, we tested the possibility that this was an obligatory first step in K^+ channel segregation. We considered a simple model in which the sequence: none → nodal → paranodal → juxtaparanodal, with reaction rates k_1, k_2, and k_3 respectively, represented a series of irreversible first order reactions. The kinetic equations were solved and a best fit (by eye) obtained with $k_1 = 0.15\ d^{-1}$, $k_2 = 0.70\ d^{-1}$, and $k_3 = 0.06\ d^{-1}$, i.e., the transition nodal → paranodal about five times faster than the initial clustering at the node. Results are plotted in Figure 3*D*. This scheme is clearly vastly oversimplified, but a comparison with the data in Figure 3*A* demonstrates that the fact that the nodal category never included >20% of the observed sites and was highly transient does not rule it out as an essential step.

DISCUSSION

When a rat is born, axons in the peripheral nervous system are in a very immature state. Schwann cells are associated with these fibers but are not yet committed to myelination. Action potentials propagate but at very slow velocity. Signals are blocked by TTX, indicating that they are mediated by Na^+ channels. However, the latter are present at very low density because they are not detected by an antibody that recognizes all known vertebrate voltage-dependent Na^+ channels. The Shaker group K^+ channel subtypes Kv1.1 and Kv1.2 are similarly not detected by immunocytochemistry. Two months later, these axons are very different. Fibers >1 μm in diameter are typically wrapped by more than 35 lamellae of tightly compacted myelin. Na^+ and K^+ channels are strongly segregated at high density within the nodal gap and the juxtaparanodes, respectively, and at much lower levels in the internodal axolemma (Shrager, 1989). Action potential conduction has changed from a continuous to a saltatory mode and has increased in velocity by one to two orders of magnitude. A remarkable feature of this progression is that axons must continue to function throughout this period, including all intermediate stages, with high stability and reliability. This study suggests that the changing distribution of K^+ channels plays an essential role in achieving this goal.

The clustering of K^+ channels is temporally and spatially distinct from that of Na^+ channels. Segregation of Na^+ channels is seen as soon as adherent Schwann cells reach the state of ensheathement (~1.5 wraps), characterized by MAG expression (Vabnick et al., 1996). This begins as early as P1 and is primarily complete by the end of the first postnatal week. By P7, there are large numbers of presumptive nodes, each with a focal cluster of Na^+ channels centered in the nodal gap. However, at this time, Kv1.1 and Kv1.2 channels are detected in only a small fraction of these sites. K^+ channel clusters are associated with large numbers of nodes only after P10. Further, in most of these sites K^+ channel immunoreactivity is detected first in paranodal regions, and only later there is a progressive transition to the juxtaparanode. This maturation is about half complete after 1 month, but continues even beyond 2 months, the latest developmental period studied here.

Over P2–P9, K^+ channel immunoreactivity was present within the nodal gap in a fraction of sites. Could this expression represent an essential stage in K^+ channel clustering? Our calculations left this possibility open by demonstrating that a simple kinetic scheme could describe the results. One outcome argues against this sequence. In Figure 1*G*, a small gap in immunoreactivity could be seen between nodal and paranodal channels. If there is lateral diffusion from node to paranode then we would expect to see a continuous gradient of fluorescence in this region. On the other hand, it may be that, as for Na^+ channel clustering during development, the level of expression at a particular locus is dependent on the relative rates of synthesis–insertion versus glial differentiation. In fibers in which the latter is relatively late, K^+ channels may appear first at the node. During remyelination, adult fibers have a significant reserve of K^+ channels in the internodal axolemma (Shrager, 1988, 1989), and clustering at newly forming nodes may thus be rapid. In remyelinating axons, nodal Kv1.1/Kv1.2 channels strongly blocked conduction, as judged by improvement effected by 4-AP (Rasband et al., 1998), and development may therefore proceed in a manner designed to minimize the likelihood of this configuration.

The spatial and temporal changes in K^+ channel distribution that occur during development suggest that maturation of the axoglial junctions may play an important role. These structures link the terminal Schwann cell loops with the axolemma. They are formed by transverse bands consisting of parallel rows of intramembranous particles in glial and axonal membranes, some of which may bridge the gap and interact to form bars of electron-dense intercellular material (Schnapp et al., 1976; Wiley and Ellisman, 1980; Tao-Cheng and Rosenbluth, 1983; Yamamoto et al., 1996). At these regions, the gap between glial and axonal membranes is reduced to just 20–30 Å. The formation of axoglial junctions in the PNS during development parallels the progressive localization of K^+ channels in the paranodes and juxtaparanodes. At the time of initial Schwann cell adhesion, junctions are not found (Tao-Cheng and Rosenbluth, 1983). At approximately P10, axoglial junctions form preferentially at terminal loops closest to the node. Over the next few weeks, they appear in increasingly more of the paranode, and by P31 almost all terminal loops are involved (Yamamoto et al., 1996). Of interest here is the fact that this is remarkably similar to the time course of sequestration of K^+ channels in the juxtaparanode, as shown in Figure 3*A*. It is thus strongly suggestive of a mechanism in which K^+ channels are excluded from regions of axoglial junctions and thereby directed to adjacent areas. A similar mechanism was proposed by Rosenbluth (1988) based on numerous measurements of intramembranous particle patches seen in freeze-fracture. Axoglial junction formation is not, however, likely to account for initial Na^+ channel clustering, which occurs as early as P1, nor can it be the sole mechanism of K^+ channel localization, because these channels are likewise absent from the nodal gap in mature fibers.

Further evidence for the influence of paranodal maturation in K^+ channel clustering is provided by our measurements of asymmetrical distributions. At 2–3 weeks of age, as many as 42% of sites were characterized by paranodal K^+ channels confined to the distal side, but by P30 this value was decreased to ~10%. In ultrastructural studies of rat sciatic nerves at P2–P12, up to two-thirds of nodes developed asymmetrically, with one paranode much more differentiated than the other (Allt, 1969; Tao-Cheng and Rosenbluth, 1983). (In these studies, proximal vs distal sidedness was not determined.) In the adult, paranodes are generally symmetric (Tao-Cheng and Rosenbluth, 1983). In developing rat spinal roots (P0–P14), on the other hand, most nodes developed with symmetry, and only occasional asymmetric sites were seen (Wiley-Livingston and Ellisman, 1980). Correspondingly, we found very few examples of asymmetrical clustering of K^+ channels in dorsal and ventral roots.

The role of K^+ channels in signal propagation

Our data indicate that the function of Kv1.1 and Kv1.2 channels varies during development in parallel with the progression described above for the anatomical localization of the channels and indeed with changes in the overall architecture of the myelinating nerve. The functional significance of these channels appears to move through three distinct stages corresponding to the early axons in which paranodes have not yet formed, transitional fibers with paranodes in the process of formation, and adult nerves in which myelination is advanced and paranodes are mature. During the early period (P0–P10), K^+ channels are directly involved in action potential generation, speeding repolarization, and decreasing the refractory period to allow trains at high frequency. During this time, Kv1.1 and Kv1.2 immunoreactivity is not detected in most axons but is present at nodal and paranodal zones in 10–20% of fibers. Because almost all axons are sensitive to 4-AP, K^+ channels are likely to be present in all cases but primarily at densities too low for detection with immunocytochemistry.

Perhaps the most striking role of K^+ channels occurs at 2–6 weeks of age, when they function to prevent bursting behavior in response to a single stimulus. This period corresponds closely to the presence of K^+ channels within paranodes. Our results suggest that it is specifically this intermediate level of maturity that is susceptible to repetitive firing. If the longitudinal resistance in the periaxonal space within the paranodes is low, as at very early times, then the delay in "reflection" of the depolarization from the next node is so short that the nodal Na^+ channels are inactivated and cannot fire again. At later stages, as axoglial junctions develop and the longitudinal resistance increases, internodal Na^+ channels become electrically isolated and cannot trigger a regenerative response at the node. Simultaneously, K^+ channels become increasingly sequestered in the juxtaparanodes, reducing or eliminating a direct involvement in action potential generation and rendering the function of these channels at this stage unclear. Alterations in Kv1.1 in the PNS have been linked to episodic ataxia–myokymia (Browne et al., 1994; Adelman et al., 1995; Smart et al., 1998). K^+ channels may also play an important protective role during injury or disease. Although conduction block is the most serious clinical consequence of demyelination, there are also "positive" neurological symptoms, including pain

and paresthesia, that result from hyperexcitability. Foci of demyelination have been shown to serve as origins of ectopic impulses or of multiple spikes evoked from single stimuli (Howe et al., 1976; Smith and McDonald, 1980; Calvin et al., 1982). Particularly noteworthy is the finding that at these sites K^+ channel block exacerbates this spontaneous discharge (Burchiel and Russell, 1985; Baker and Bostock, 1992), and therapeutic attempts to restore conduction must therefore be balanced to avoid introducing hyperexcitability. Thus, during disease, K^+ channels may recapitulate their developmental function to stabilize conduction while the passive electrical properties of the axon are undergoing major transformations.

REFERENCES

Adelman JP, Bond CT, Pessia M, Maylie J (1995) Episodic ataxia results from voltage dependent potassium channels with altered functions. Neuron 15:1449–1454.

Allt G (1969) Ultrastructural features of the immature peripheral nerve. J Anat 105:283–293.

Baker M, Bostock H (1992) Ectopic activity in demyelinated spinal root axons of the rat. J Physiol (Lond) 451:539–552.

Barrett EF, Barrett JN (1982) Intracellular recording from vertebrate myelinated axons: mechanism of the depolarizing afterpotential. J Physiol (Lond) 323:117–144.

Bekele-Arcuri Z, Matos MF, Manganas MM, Strassle BW, Monaghan MM, Rhodes KJ, Trimmer JS (1996) Generation and characterization of subtype-specific monoclonal antibodies to K^+ channel alpha and beta subunit polypeptides. Neuropharmacology 35:851–865.

Bowe CM, Kocsis JD, Waxman SG (1985) Differences between mammalian ventral and dorsal spinal roots in response to blockade of potassium channels during maturation. Proc R Soc Lond Ser B 224:355–366.

Browne DL, Gancher ST, Nutt JG, Brunt ERP, Smith EA, Kramer P, Litt M (1994) Episodic ataxia/myokymia syndrome is associated with point mutations in the human potassium channel gene, KCNA1. Nat Genet 8:136–140.

Burchiel KJ, Russell LC (1985) Effects of potassium channel-blocking agents on spontaneous discharges from neuromas in rats. J Neurosurg 63:246–249.

Calvin WH, Devor M, Howe JF (1982) Can neuralgias arise from minor demyelination? Spontaneous firing, mechanosensitivity, and afterdischarge from conducting axons. Exp Neurol 75:755–763.

Chiu SY, Ritchie JM (1981) Evidence for the presence of potassium channels in the paranodal region of acutely demyelinated mammalian single nerve fibres. J Physiol (Lond) 313:415–437.

Chiu SY, Ritchie JM (1982) Evidence for the presence of potassium channels in the internode of frog myelinated nerve fibres. J Physiol (Lond) 322:485–501.

Chiu SY, Ritchie JM (1984) On the physiological role of internodal potassium channels and the security of conduction in myelinated nerve fibres. Proc R Soc Lond Ser B 220:415–422.

Chiu SY, Ritchie JM, Rogart RB, Stagg D (1979) A quantitative description of membrane currents in rabbit myelinated nerve. J Physiol (Lond) 292:149–166.

Dodge F, Frankenhaeuser B (1958) Membrane currents in isolated frog nerve fibre under voltage clamp conditions. J Physiol (Lond) 143:76–90.

Dugandzija-Novakovic S, Koszowski AG, Levinson SR, Shrager P (1995) Clustering of Na channels and node of Ranvier formation in remyelinating axons. J Neurosci 15:492–502.

Fields RD, Black JA, Bowe CM, Kocsis JD, Waxman SG (1986) Differences in intramembranous particle distribution in the paranodal axolemma are not associated with functional differences of dorsal and ventral roots. Neurosci Lett 67:13–18.

Frankenhaeuser B, Huxley AF (1964) The action potential in the myelinated nerve fibre of *Xenopus laevis* as computed on the basis of voltage clamp data. J Physiol (Lond) 171:302–315.

Grissmer S, Nguyen AN, Aiyar J, Hanson DC, Mather RJ, Gutman GA, Karmilowicz MJ, Auperin DD, Chandy KG (1994) Pharmacological characterization of five cloned voltage-gated K^+ channels, types Kv1.1, 1.2, 1.3, 1.5, and 3.1, stably expressed in mammalian cell lines. Mol Pharmacol 45:1227–1234.

Hille B (1967) The selective inhibition of delayed potassium currents in nerve by tetraethylammonium ion. J Gen Physiol 50:1287–1302.

Hines M, Carnevale NT (1997) The NEURON simulation. Neural Comput 9:1179–1209.

Hopkins WF, Allen ML, Houamed KM, Tempel BL (1994) Properties of voltage-gated K^+ currents expressed in *Xenopus* oocytes by mKv1.1, mKv1.2 and their heteromultimers as revealed by mutagenesis of the dendrotoxin-binding site in mKv1.1. Pflügers Arch 428:382–390.

Howe JF, Calvin WH, Loeser JD (1976) Impulses reflected from dorsal root ganglia and from focal nerve injuries. Brain Res 116:139–144.

Kocsis JD, Ruiz JA, Waxman SG (1983) Maturation of mammalian myelinated fibers: changes in action-potential characteristics following 4-aminopyridine application. J Neurophysiol 50:449–463.

Martini R, Schachner M (1986) Immunoelectron microscopic localization of neural cell adhesion molecules (L1, N-CAM, and MAG) and their shared carbohydrate epitope and myelin basic protein in developing sciatic nerve. J Cell Biol 103:2439–2448.

Mi H, Deerinck TJ, Ellisman MH, Schwarz TL (1995) Differential distribution of closely related potassium channels in rat Schwann cells. J Neurosci 15:3761–3774.

Milton RL, Mathias RT, Eisenberg RS (1985) Electrical properties of the myotendon region of frog twitch muscle fibers measured in the frequency domain. Biophys J 48:253–267.

Polman CH, Hartung HP (1995) The treatment of multiple sclerosis: current and future. Curr Opin Neurol 8:200–209.

Poltorak M, Sadoul R, Keilhauer G, Landa C, Fahrig T, Schachner M (1987) Myelin-associated glycoprotein, a member of the L2/HNK-1 family of neural cell adhesion molecules, is involved in neuron–oligodendrocyte and oligodendrocyte–oligodendrocyte interaction. J Cell Biol 105:1893–1899.

Rasband MN, Trimmer JS, Schwarz TL, Levinson SR, Ellisman MH, Schachner M, Shrager P (1998) Potassium channel distribution, clustering, and function in remyelinating rat axons. J Neurosci 18:36–47.

Rhodes KJ, Monaghan MM, Barrezueta NX, Nawoschik S, Bekele-Arcuri Z, Matos MF, Nakahira K, Schechter LE, Trimmer JS (1996) Voltage-gated K^+ channel beta subunits: expression and distribution of Kv beta 1 and Kv beta 2 in adult rat brain. J Neurosci 16:4846–4860.

Rhodes KJ, Strassle BW, Monaghan MM, Bekelearcuri Z, Matos MF, Trimmer JS (1997) Association and colocalization of the Kv-beta-1 and Kv-beta-2 beta subunits with Kv1 alpha subunits in mammalian brain K^+ channel complexes. J Neurosci 17:8246–8258.

Roper J, Schwarz JR (1989) Heterogeneous distribution of fast and slow potassium channels in myelinated rat nerve fibres. J Physiol (Lond) 416:93–110.

Rosenbluth J (1988) Role of glial cells in the differentiation and function of myelinated axons. Int J Dev Neurosci 6:3–24.

Schmidt H, Stampfli R (1966) Die wirkung von tetraathylammoniumchlorid auf den einzelnen ranvierschen schnurring. Pflügers Arch 287:311–325.

Schnapp B, Peracchia C, Mugnaini E (1976) The paranodal axo-glial junction in the central nervous system studied with thin sections and freeze-fracture. Neuroscience 1:181–190.

Schwid SR, Petrie MD, McDermott MP, Tierney DS, Mason DH, Goodman AD (1997) Quantitative assessment of sustained-release 4-aminopyridine for symptomatic treatment of multiple sclerosis. Neurology 48:817–821.

Sheng M, Tsaur ML, Jan YN, Jan LY (1992) Subcellular segregation of two A-type K^+ channel proteins in rat central neurons. Neuron 9:271–284.

Sheng M, Tsaur ML, Jan YN, Jan LY (1994) Contrasting subcellular localization of the Kv1.2 K^+ channel subunit in different neurons of rat brain. J Neurosci 14:2408–2417.

Sherratt RM, Bostock H, Sears TA (1980) Effects of 4-aminopyridine on normal and demyelinated mammalian nerve fibres. Nature 283:570–572.

Shi G, Nakahira K, Hammond S, Rhodes KJ, Schechter LE, Trimmer JS (1996) Beta subunits promote K^+ channel surface expression through effects early in biosynthesis. Neuron 16:843–852.

Shrager P (1987) The distribution of sodium and potassium channels in single demyelinated axons of the frog. J Physiol (Lond) 392:587–602.

Shrager P (1988) Ionic channels and signal conduction in single remyelinating frog nerve fibres. J Physiol (Lond) 404:695–712.

Shrager P (1989) Sodium channels in single demyelinated mammalian axons. Brain Res 483:149–154.

Smart SL, Lopantsev V, Zhang CL, Robbins CA, Wang H, Chiu SY, Schwartzkroin PA, Messing A, Tempel BL (1998) Deletion of the Kv1.1 potassium channel causes epilepsy in mice. Neuron 20:809–819.

Smith KJ, McDonald WI (1980) Spontaneous and mechanically evoked activity due to central demyelinating lesion. Nature 286:154–155.

Stampfli R (1952) Bau und funktion isolierter markhaltiger nervenfasern. Ergeb Physiol Biol Chem Exp Pharmakol 47:70–165.

Strichartz GR, Small RK, Pfenninger KH (1984) Components of the plasma membrane of growing axons. III. Saxitoxin binding to sodium channels. J Cell Biol 98:1444–1452.

Stys PK, Ransom BR, Waxman SG (1991) Compound action potential of nerve recorded by suction electrode: a theoretical and experimental analysis. Brain Res 546:18–32.

Swanson R, Marshall J, Smith JS, Williams JB, Boyle MB, Folander K, Luneau CJ, Antanavage J, Oliva C, Buhrow SA, Bennett C, Stein RB, Kaczmarek LK (1990) Cloning and expression of cDNA and genomic clones encoding three delayed rectifier potassium channels in rat brain. Neuron 4:929–939.

Tao-Cheng JH, Rosenbluth J (1982) Development of nodal and paranodal membrane specializations in amphibian peripheral nerves. Brain Res 255:577–594.

Tao-Cheng JH, Rosenbluth J (1983) Axolemmal differentiation in myelinated fibers of rat peripheral nerves. Brain Res 285:251–263.

Trimmer JS, Trowbridge IS, Vacquier VD (1985) Monoclonal antibody to a membrane glycoprotein inhibits acrosome reaction and associated Ca^{++} and H^+ fluxes of sea urchin sperm. Cell 40:697–703.

Vabnick I, Shrager P (1998) Ion channel redistribution and function during development of the myelinated axon. J Neurobiol 37:80–96.

Vabnick I, Novakovic SD, Levinson SR, Schachner M, Shrager P (1996) The clustering of axonal sodium channels during development of the peripheral nervous system. J Neurosci 16:4914–4922.

Wang H, Kunkel DD, Martin TM, Schwartzkroin PA, Tempel BL (1993) Heteromultimeric K^+ channels in terminal and juxtaparanodal regions of neurons. Nature 365:75–79.

Webster HD (1971) The geometry of peripheral myelin sheaths during their formation and growth in rat sciatic nerves. J Cell Biol 48:348–367.

Wiley CA, Ellisman MH (1980) Rows of dimeric-particles within the axolemma and juxtaposed particles within glia, incorporated into a new model for the paranodal glial-axonal junction at the node of Ranvier. J Cell Biol 84:261–280.

Wiley-Livingston C, Ellisman MH (1980) Development of axonal membrane specializations defines nodes of Ranvier and precedes Schwann cell myelin elaboration. Dev Biol 79:334–355.

Yamamoto K, Merry AC, Sima AA (1996) An orderly development of paranodal axoglial junctions and bracelets of Nageotte in the rat sural nerve. Dev Brain Res 96:36–45.

Ziskind-Conheim L (1988) Physiological and morphological changes in developing peripheral nerves of rat embryos. Dev Brain Res 42:15–28.